2001-07-30

Frequency Response of Pressure Sensor Configurations in Slip-Flow Conditions

Whitmore, Stephen A.

American Institute of Aeronautics & Astronautics

Whitmore, Stephen A. "Frequency response of pressure sensor configurations in slip-flow conditions." Journal of spacecraft and rockets 39.2 (2002): 219-226. http://hdl.handle.net/10945/69330

JOURNAL OF SPACECRAFT AND ROCKETS
Vol. 39, No. 2, March–April 2002

Frequency Response of Pressure Sensor Configurations in Slip-Flow Conditions

Stephen A. Whitmore*
Naval Postgraduate School, Monterey, California 93943

A dynamic model is presented for pneumatic tubing and pressure sensor configurations in rarefied or slip-flow conditions. The model uses the linearized Navier–Stokes equations, with the boundary conditions extended to allow for rarefied conditions. At low pressure levels, the modified wall boundary condition allows fluid elements to slip when directly in contact with the tubing wall. This slippage effectively lowers fluid viscosity. Dynamic effects of the rarefied-flow extension are demonstrated by comparing rarefied-flow solutions to equivalent solutions generated using continuum-flow models. Lower viscosity resulting from rarefied flow causes the configuration response to be less damped than for similar conditions without molecular effects. Comparing steady-state response to data from a series of laboratory experiments validates the range of the rarefied-flow model. When pneumatic tubing is heated unevenly, rarefied flow forces the tube hot end to have higher pressure than the cold end, with no net flow along the tube. This pressure difference results in a dc offset in the measured pressure reading. Comparisons of the steady-state model to experimental data show that the slip-flow model is generally applicable for Knudsen numbers up to approximately 0.65. Beyond 0.7 Knudsen number, molecular effects dominate, and the model is no longer applicable to the problem physics.

Nomenclature

A_c	=	tube cross-sectional area, cm^2 (in.^{2})
c	=	sonic velocity, m/s (ft/s)
d	=	tube diameter, cm (in.)
i	=	node index
J_0	=	zeroth-order Bessel function
J_1	=	first-order Bessel function
J_2	=	second-order Bessel function
j	=	$\sqrt{-1}$
K	=	polytropic density proportionality constant
K_M	=	Maxwell pressure parameter
L	=	tube length, cm (in.)
n	=	number of computational nodes
P	=	pressure, kPa (μm of Hg, psf)
P_{cold}	=	pressure at cold end of tube, kPa (μm of Hg, psf)
P_{hot}	=	pressure at hot end of tube, psf
P_I	=	pressure at transducer, kPa (μm of Hg, psf)
Pr	=	Prandtl number
P_0	=	pressure at surface, kPa (μm of Hg, psf)
$P_{1,2,3,\ldots,n}$	=	pressure at computational nodes 1, 2, 3, . . . , n, kPa (μm of Hg, psf)
P_∞	=	ambient pressure, kPa (psf)
R	=	tube radius, cm (in.)
R_g	=	universal gas constant, Nt-m/kg K (ft-lbf/[lbm °R])
r	=	radial coordinate, cm (in.)
T	=	temperature, °C (°F)
T_{cold}	=	temperature at cold end of tube, °C (°F)
T_{hot}	=	temperature at hot end of tube, °C (°F)
T_∞	=	ambient temperature, °C (°F)
t	=	time, s
U	=	longitudinal velocity, m/s (ft/s)
U_{creep}	=	creep flow velocity at tubing wall, m/s (ft/s)
U_{slip}	=	slip velocity at the wall, m/s (ft/s)
U_{wall}	=	total longitudinal velocity at wall, m/s (ft/s)
V	=	transducer volume, cm^3 (in.^{3})
V_e	=	effective volume of a model node, cm^3 (in.^{3})
x	=	longitudinal coordinate, cm (in.)
α	=	shear wave number, $j^{3/2}\sqrt{(\omega\rho_0 R^2/\mu_0)}$
Γ_p	=	wave propagation factor
ΔT_{random}	=	random error in temperature, measurement, °C (°F)
δP_{McLeod}	=	rms error in McLeod gauge measurement, kPa (psf)
$\delta P_{\text{Vernier}}$	=	rms error in Vernier manometer measurement, kPa (psf)
$\partial P/\partial x$	=	longitudinal pressure gradient, kPa/m (psf/ft)
$\partial T/\partial x$	=	longitudinal temperature gradient, K/m (°F/ft)
$\partial U/\partial r$	=	velocity shear at wall [m/s] · cm ([ft/s] · in.)
ε	=	ratio of slip distance to mean free path
ϑ	=	slip distance, μm
κ	=	Knudsen number
κ_p	=	rarefied-flow correction term in momentum equation
κ_0	=	Knudsen number based on mean flow properties
Λ	=	first-variation operator
ΛT	=	rms error in temperature measurement, °C (°F)
λ	=	mean free path of the fluid molecules, μm
μ	=	dynamic viscosity, kg · [m/s] (lbm · [ft/s])
μ_0	=	local steady-state bulk viscosity in the tubing, kg · [m/s] (lbm · [ft/s])
ξ	=	polytropic expansion parameter
π	=	irrational constant, 3.1415926535898 . . .
ρ	=	density, kg/m^3 (lbm/ft^3)
ρ_0	=	density based on mean flow properties, kg/m^3 (lbm/ft^3)
Ψ^2	=	mean-squared error
ω	=	radian frequency, 1/s
$20\log\|\cdot\|$	=	log-magnitude of a complex quantity, dB

Received 14 February 2001; revision received 27 July 2001; accepted for publication 30 July 2001.

*Michael J. Smith Space Systems NASA Chair, Space Systems Academic Group. Associate Fellow AIAA.

Introduction

ACHIEVING the ability to sense surface pressures accurately on hypersonic or flight vehicles presents a formidable measurement challenge. The hostility of the sensing environment precludes intrusion into the flow, and measurements must be obtained using significant lengths of small-diameter pneumatic tubing to connect the surface ports to remotely located pressure transducers. An idealized pneumatic configuration is shown in Fig. 1 and consists of a

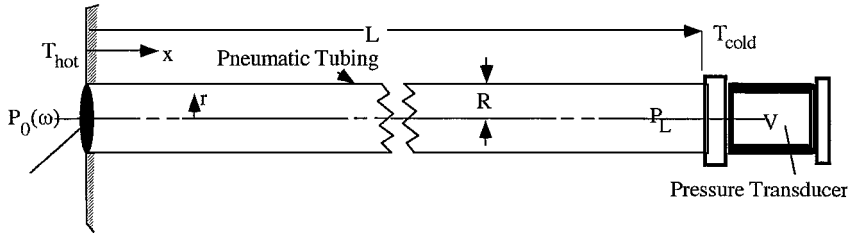

Fig. 1 Idealized schematic of pressure sensor configuration.

surface pressure port connected to a pressure transducer using a section of cylindrical pneumatic tubing. The pneumatic tubing has a diameter D (radius R) and length L. A small volume V is attached to the downstream end of the tubing to represent the entrapped volume of the pressure transducer.

Away from the stagnation regions on the vehicle, in hypersonic-flow regimes pressure levels to be sensed are generally very low. For some applications, such as air data measurements, local surface static pressure levels are as low as 0.001 atm (0.1 kPa). Further complicating the sensing problem is the effect of viscous boundary-layer heating at the surface. This surface heating requires the surface port to be very small and also induces large temperature gradients along the length of the pneumatic tubing. Because of the combination of very low pressure levels, small-diameter pneumatic lines, and large temperature gradients, molecular effects are no longer negligible

Background

The basic problem of predicting tube-flow dynamics has been extensively studied. For continuum-flow conditions, Lamb,[1] Iberall,[2] Schuder and Binder,[3] and Hougen et al.[4] have developed closed-form frequency-domain solutions for simple tubing geometries and constant wall temperatures. Berg and Tijdeman[5] and Tijdeman[6] extend the analyses of Schuder and Binder[3] and Hougen et al.[4] to develop a recursion formula for a complex geometry, which consists of cascades of tubes and volumes. Parrot and Zorumski[7] investigated the dynamic transmission of sound in a simple quartz tube subjected to high temperatures and large longitudinal temperature gradients. References 1–7 are valid only for continuum-flow conditions. Maxwell,[8] Knudsen,[9] and Tompkins and Wheeler[10] have investigated tube flow for rarefied conditions at high temperatures with longitudinal temperature gradients. However, these rarefied flow investigations considered only steady-flow conditions. The effects of time-varying pressure input conditions were not investigated.

The dynamic influence of rarefied flow phenomena on pneumatic pressure sensing systems has not been generally well understood; consequently, research was initiated at the NASA Dryden Flight Research Center with a primary objective to develop a dynamic response model for pneumatic pressure sensing systems that is applicable to both continuum and rarefied flows. Whitmore et al.[11] present a detailed analytical development and empirical validation of one such model.

For completeness, this paper summarizes information presented in detail in Ref. 11. Additionally, this paper presents frequency-response analyses for intermediate-Knudsen-number flow conditions not presented in Ref. 11. Also, additional laboratory data not available when Ref. 11 was originally published will be presented. These additional data will be compared to data taken from Ref. 11. The new data to be presented directly support the conclusions drawn by the authors in Ref. 11. The model provides fundamental insight into the behavior of longitudinal pressure waves at the transition between continuum and rarefied flow. Additionally, the model provides instrumentation designers with a tool that can be used to predict and evaluate the responses of complex pneumatic systems over a wide range of flow conditions that vary continuously from continuum to slip flow.

Mathematical Analysis

In this paper, the model of Berg and Tijdeman[5] and Tijdeman[6] is extended to allow for rarefied conditions by modifying the wall boundary condition to allow fluid elements to move when directly in contact with the wall. This boundary condition contrasts to the classical no-slip condition used for continuum-flow mechanics. Other than the wall boundary condition modification, the classical equations of fluid motion fully apply in the slip-flow regime.

Slip-flow conditions correspond to flow regimes with values of Knudsen number that lie between approximately 0.01 and 1.0. For hypersonic, reentry, and suborbital flight applications, Knudsen numbers variations from zero to approximately 0.50 are typically encountered. For typical orbital applications, the flow is so rarefied that the Navier–Stokes equations no longer model the physics of the flow. For these applications one must resort to statistical thermodynamics to model the fluid behavior.[8–10]

Knudsen Number

The Knudsen number is defined as the ratio of the average distance each fluid particle travels between collisions (the mean free path distance λ) and the characteristic length scale of the system. If the length scale of the system is defined to be the tube radius R, the Knudsen number can be approximated by the expression[12]

$$\kappa \approx \sqrt{R_g \pi T}(\mu/RP) \tag{1}$$

In Eq. (1) T is the local gas temperature.

Modified Wall Boundary Condition

For slip-flow conditions, the fluid velocity at the wall can be decomposed into two parts,[12] the wall slip velocity and the thermomolecular creep velocity. The wall slip velocity is a result of reduced wall fluid viscosity in rarefied flow conditions. Fluid molecules no longer stick to the walls of the tube, but instead slide along the wall. The thermomolecular creep is a transpiration phenomenon where the fluid molecules in contact with the heated tubing wall actually migrate from the hot end of the tube toward the colder end. The modified wall boundary condition is the sum of the slip and molecular creep velocities. The slip velocity is proportional to the local wall shearing stress, but in the opposite direction:

$$U_{\text{slip}} = -\vartheta \frac{\partial U}{\partial r} \tag{2a}$$

In Eq. (2a) ϑ is defined as the slip distance and is an empirical parameter that accounts for reduced fluid viscosity in rarefied flow conditions. The ratio of slip distance to the mean free path λ is defined as

$$\varepsilon = \vartheta/\lambda$$

For the analyses presented, ε is assumed to have a magnitude of approximately 1.0. The unity value is a good approximation for metallic surfaces. For ceramic surfaces, the magnitude of ε is a bit larger. For example, quartz glass has an ε value of approximately 1.25. Kennard[12] has tabulated values of ε for various materials of interest for high-temperature or high-speed flight applications.

The molecular creep velocity is proportional to the local longitudinal temperature gradient and inversely proportional to the local pressure. Molecular creep is caused by gas molecules originating from the hot end of the tube having higher kinetic energy than molecules originating from the colder regions. The result is that the hot-end molecules recoil from collisions more strongly than do cold-end molecules, and gas molecules at the wall acquire a net tangential momentum toward the hot end of the tube. Consequently, fluid molecules creep along the tubing walls with a velocity that is directly proportional to the local temperature gradient:

$$U_{\text{creep}} = \frac{3}{4}\frac{\mu_0 R_g}{P_0}\frac{\partial T}{\partial x} \tag{2b}$$

Summing Eqs. (2a) and (2b), the resulting equation for the modified boundary condition is

$$U_{\text{wall}}(x,t) = U_{\text{creep}} + U_{\text{slip}} = \frac{3}{4}\frac{\mu_0 R_g}{P_0}\frac{\partial T}{\partial x} - \vartheta\frac{\partial U}{\partial r} \tag{3}$$

In Eq. (3), μ_0 and P_0 are the longitudinal averages of viscosity and pressure.

Solving the Boundary Value Equations

When the procedure laid out by Berg and Tijdeman[5] and Tijdeman[6] is followed, the Navier–Stokes equations, expressed in cylindrical coordinates, are linearized using small perturbations. The linearized boundary value equations express the pressure, temperature, and velocity within the tube as a function of time t, radial distance from the center of the tube r, and longitudinal location x in the tube.

The energy equation is decoupled from the momentum and continuity equations by assuming the wave expansion process in the tube to be polytropic. A polytropic process is a simple energy model that relates pressure, temperature, and density[13,14]:

$$P = K\rho^{\xi} \tag{4}$$

The polytropic expansion parameter ξ has limiting values given by $1 < \xi \leq \gamma$, where γ is the ratio of specific heats at constant pressure and volume. Values of $\xi = \gamma$ correspond to an isentropic expansion. For values of $\xi < \gamma$, the expansion process is irreversible. A value of $\xi = 1$ corresponds to a constant temperature process. The decoupling process implicitly expresses the temperature within the tube as a function of pressure and velocity.

The resulting linearized and temperature-decoupled boundary value equations are averaged across the radius of the tube to give a set of one-dimensional partial differential equations where the pressure and velocity in the tube vary as a function of t and x. When the Fourier transforms of the radial-averaged boundary value equations are evaluated, the partial differential equations with respect to t and x are transformed to ordinary differential equations with respect to x. The frequency-domain boundary value equations now have the radian frequency of the longitudinal pressure wave in the tube ω as a fundamental parameter. If one assumes that gas properties and tube diameter remain constant along the length of the tube, the one-dimensional, frequency-domain boundary value problem can be solved analytically. This fundamental solution is used as a building block for complex solutions where fluid properties and tubing geometry are allowed to change longitudinally along the length of the tube.

Complex solutions can be achieved by starting at the transducer end (Fig. 1) of the tube and analytically integrating upstream over an incremental length (finite element). A solution node is defined as the point where the boundary conditions of one finite element must mesh with the boundary conditions of another element. The problem is solved recursively assuming n solution nodes starting at the transducer end (nth node) and working toward the surface end (0th node) of the tube. Using these recursive formulas, solutions for arbitrary geometries and longitudinal temperature profiles are constructed.

Recursion Formulas

The resulting recursive formulas for the frequency response, the ratio of the Fourier transform of pressure at the transducer end of the tube to the Fourier transform of the pressure at the surface end of the tube, is

$$\frac{P_L(\omega)}{P_0(\omega)} = \frac{P_1(\omega)}{P_0(\omega)}\frac{P_2(\omega)}{P_1(\omega)}\cdots\frac{P_{n-1}(\omega)}{P_{n-2}(\omega)}\frac{P_n(\omega)}{P_{n-1}(\omega)}$$
$$= \prod_{i=1}^{n}\left(1\Big/\left\{\cosh\left[\omega\Gamma_{p_i}\frac{L_i}{c_i}\right] + \omega\frac{V_{e_i}\Gamma_{p_i}}{A_{c_i}c_i}\sinh\left[\omega\Gamma_{p_i}\frac{L_i}{c_i}\right]\right\}\right) \tag{5}$$

In Eq. (5), the parameter V_{e_i} is the effective volume and accounts for the entrapped volume at the ith node plus the impedance of all downstream tubes and volumes. At the nth node there are no downstream impedances, and V_n is only the volume entrapped by the pressure transducer. The recursion formulas for the V_e are

$$V_{e_i} = V_i + \frac{\left(c_i^2/c_{i+1}^2\right)V_{e_{i+1}}\{\cosh[\omega\delta_{i+1}] + [1/(\omega\eta_{i+1})]\sinh[\omega\delta_{i+1}]\}}{\cosh[\omega\delta_{i+1}] + \omega\eta_{i+1}\sinh[\omega\delta_{i+1}]} \tag{6}$$

where

$$\eta_{i+1} = \Gamma_{p_{i+1}}\frac{V_{e_{i+1}}}{A_{c_{i+1}}c_{i+1}} \tag{7a}$$

$$\delta_{i+1} = \Gamma_{p_{i+1}}\frac{L_{i+1}}{c_{i+1}} \tag{7b}$$

$$\Gamma_p = \left\{\frac{(\gamma/\xi)[J_0[\alpha] - \vartheta(\alpha/R)J_1[\alpha]]}{\kappa_p(J_2[\alpha] + \vartheta(\alpha/R)J_1[\alpha]) + j\omega\frac{3}{4}(\mu/\bar{P}_0)[(\xi-1)/\xi](2/\alpha)J_1[\alpha]}\right\}^{\frac{1}{2}} \tag{7c}$$

In Eq. (7c), Γ_p is referred to as the wave propagation factor[5,6,11] and accounts for the dissipative forces acting at the tubing walls. As developed by Berg and Tijdeman[5] and Tijdeman,[6] the variation of ξ as a function of the fundamental flow parameters is given by

$$\xi = \left[1 + \left[\frac{\gamma-1}{\gamma}\right]\frac{J_2[\sqrt{Pr}\,\alpha]}{J_0[\sqrt{Pr}\,\alpha]}\right]^{-1} \tag{7d}$$

Equation (7d) is a direct result of the polytropic process assumption made earlier [Eq. (4)]. If the rarefied flow terms are dropped from Eqs. (5–7), then algorithm exactly reduces to the recursion model developed by Berg and Tijdeman[5] and Tijdeman[6] for continuum-flow conditions.

Results and Discussion

The dynamic model presented in Eqs. (5–7) predicts that rarefied gas effects will manifest themselves primarily in two peculiar ways:

1) At very low pressure levels, low molecular density allows fluid to slip at the tubing wall. Fluid viscosity is effectively lowered, and dynamic response of the tubing configuration is less damped than occurs when molecular effects are negligible.

2) To balance creep flow at the wall, gas molecules near the tube centerline migrate from hot to cold ends of the tube. This migration establishes a pressure gradient. With no net flow in the tube, the hot end of the tube will have a higher average pressure level than does the cold end.

Slip-Flow Frequency Response

Theoretical effects of rarefied flow on frequency response are shown in Figs. 2 and 3. In Figs. 2 and 3, the frequency response of an example configuration is analyzed for ambient pressure levels from 0.00005 to 0.25 atm. The configuration parameters are $L = 30.5$ cm (12 in.), $D = 0.1585$ cm (0.0625 in.), $V = 0.08$ cm^3 (0.005 in.^{3}), and $T_{\text{amb}} = 5°\text{C}$ (500°F). Table 1 shows Knudsen numbers corresponding to the analyzed pressure levels.

In Fig. 2a, the frequency-response magnitude in decibels,

$$20\log\{\|P_L(\omega)/P_0(\omega)\|\}$$

is plotted with the rarefied-flow effects modeled. In Fig. 2b, the frequency-response magnitude in decibels is plotted without rarefied-flow effects modeled. Clearly, at the higher pressure levels where the Knudsen numbers are very low, the frequency-response curves with and without the Knudsen number effects are nearly identical. However, as the pressure drops, the model without rarefied gas

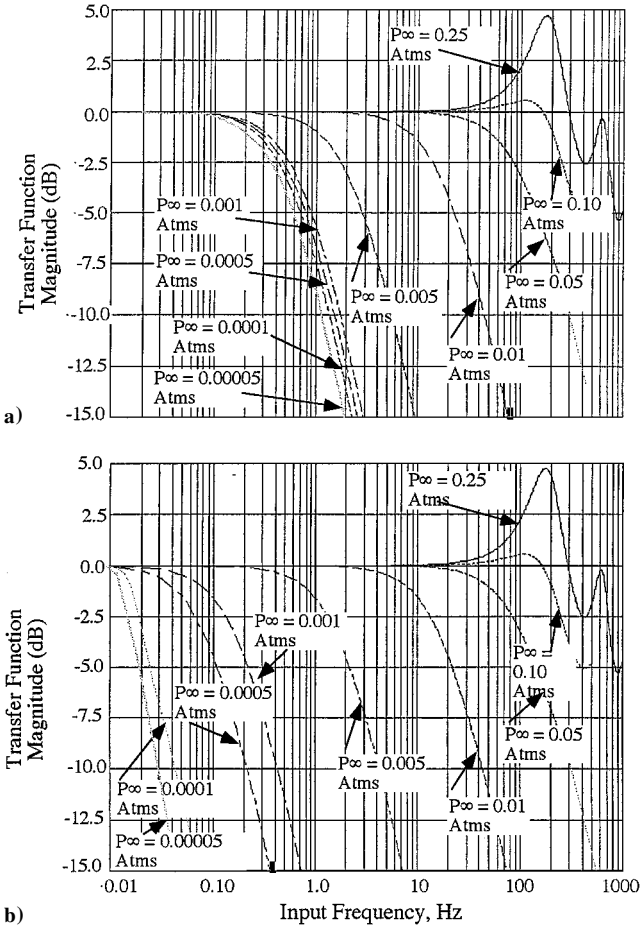

Fig. 2 Tubing frequency response for various ambient pressure levels, $L = 30.5$ cm, $D = 0.16$ cm, and $T_\infty = 5°C$: a) real gas effects modeled and b) real gas effects not modeled.

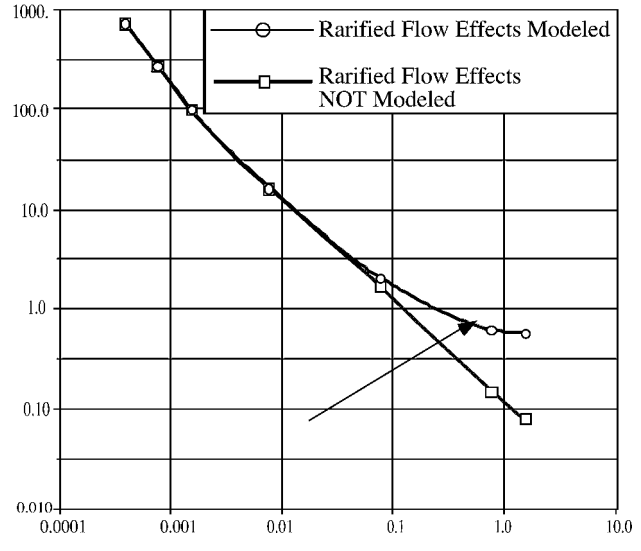

Fig. 3 Half-power frequency as function of Knudsen number.

effects exhibits significant magnitude attenuation when compared to the model with rarefied gas effects.

Figure 3 shows a summary of the results of Figs. 2a and 2b. In Fig. 3, the frequency of the half-power point (the point where the magnitude is attenuated 3 dB from the dc level) is plotted as a function of Knudsen number. The two curves are in good agreement up to approximately $\kappa = 0.05$. Beyond this point, the two curves diverge. At higher Knudsen numbers the frequency-response magnitude of the model with rarefied-gas effects is significantly less attenuated. From this result, it can be concluded that rarefied-gas fluid slip at the wall boundary has the same effect as reducing the viscosity of the fluid.

Table 1 Knudsen numbers corresponding to the analyzed pressure levels[a]

Atm	kPa	psf	κ
0.2500	25.33	529.05	3.1×10^{-4}
0.1000	10.13	211.62	7.6×10^{-4}
0.0500	5.07	105.81	1.5×10^{-3}
0.0100	1.01	21.16	7.6×10^{-3}
0.0050	0.51	10.58	1.5×10^{-2}
0.0010	0.10	2.12	7.6×10^{-2}
0.0005	0.05	1.06	0.1530
0.0001	0.01	0.21	0.7640
0.00005	0.005	0.11	1.5280

[a]Ambient pressure level.

Frequency-Response Experiments

In Ref. 11, a detailed validation is presented of the dynamic model at continuum-flow conditions for a variety of tube geometries sizable temperature gradients are forced along the lengths of the tubes. However, validation of the model frequency response for rarefied flow conditions has not been performed. The task of devising an experimental procedure to measure the dynamic response of a tubing/sensor configuration for slip-flow conditions is quite daunting.

Acoustical methods normally used to generate a controlled input signal to the sensor configuration are not applicable for extremely low pressure levels. Electromechanical actuators such as high-fidelity speaker systems require a minimal level of air impedance to function properly. The air density required to achieve this impedance level is high enough that rarefied flow effects are negligible. Similarly, without significant redesign, existing shock tunnels[15] cannot be used to generate the input pressure pulse. Fairly significant differential pressure levels are required to burst cleanly the shock-tunnel membrane that isolates the evacuated end of the tunnel from the pressurized end. The incoming pressure wave fills the evacuated space upstream of the membrane, and the resulting pressure levels become too high for rarefied gas effects to exist. All rarefied-gas and thermomolecular effects are wiped out immediately after the pulse is formed. Perhaps performing frequency-response or shock-tube types of measurements at low-to-moderate pressure levels for microdiameter tubing could offer a viable solution. The potential of using an electrical arc to generate a shock pulse should be investigated. However, in this case it must be recognized that plasma effects will occur, and these may confuse the results of the tests. In any case, development of these measurement methods were beyond the scope and funding for this research. The dynamic effects presented in Figs. 2 and 3 remain unvalidated by empirical measurements at this point and unhappily remain as a challenge for future researchers.

Steady-State Model Response at High Knudsen Numbers

In the classical work on rarefied flow,[8] Maxwell determined that in the free-molecular limit (infinite Knudsen number) the ratio of the steady-state pressure gradient, when normalized by the mean pressure level in the tube, is equal to one-half of the temperature gradient in the tube when normalized by the mean temperature in the tube:

$$\frac{\partial P/\partial x}{P} = \frac{1}{2}\frac{\partial T/\partial x}{T} \tag{8}$$

For conditions that lie somewhere between the free-molecular regime and the continuum-flow regime, the pressure gradient induced by longitudinal temperature gradients is less than the limit predicted by Maxwell and is strongly a function of Knudsen number.[1,10] Thus, it is important to examine the steady-state behavior of Eqs. (5–7) to determine that they exhibit a similar behavior.

The steady-state behavior of the dynamic model was analyzed by applying the final-value theorem[16] to Eqs. (5–7). This final-value analysis is presented in detail in Ref. 11. The normalized steady

pressure gradient can be written as a function of Knudsen number and normalized temperature gradient. The resulting expression is

$$\frac{\partial P/\partial x}{P} = \frac{\partial T/\partial x}{T}\frac{6\kappa^2}{\pi(1+4\varepsilon\kappa)} \tag{9}$$

Equation (9) predicts that for small Knudsen number a very large temperature gradient is required to get a measurable steady-state pressure gradient. However, for higher Knudsen numbers, a significant steady-state pressure gradient can occur for relatively moderate temperature gradients. Also, when it is assumed that the local Knudsen number is approximated by the longitudinally averaged Knudsen number κ_0, Eq. (9) can be integrated with respect to x to give

$$\ell n\left[\frac{P_{\text{hot}}}{P_{\text{cold}}}\right] = \ell n\left[\frac{\left(\dfrac{6\kappa_0^2}{\pi(1+4\varepsilon\kappa_0)}\right)}{\dfrac{T_{\text{hot}}}{T_{\text{cold}}}}\right] \tag{10}$$

Equation (10) demonstrates that the resulting temperature-induced pressure ratio is primarily a function of the endpoint temperatures and does not strongly depend on temperature distribution along the tube.

More important, in the free-molecule limit (infinite Knudsen number), neither Eq. (9) nor Eq. (10) approaches a finite limit as predicted by Maxwell [Eq. (8)]. Thus, one must conclude that the model of Eqs. (5–7) is not applicable in the very high-Knudsen-number flow regime. Because the Navier–Stokes equations used to model the flow in the core of the tube begin to break down at very high Knudsen numbers, this conclusion makes sense. The relevant question is, At what Knudsen number does the dynamic model begin to break down? Because Eq. (9) is directly derived from the dynamic model, the steady-state behavior provides a means for evaluating the valid Knudsen number ranges for the dynamic model. When the predictions of Eq. (9) are compared against experimental data, one can judge the validity range by looking at the point where the predictions diverge from the empirical data.

Steady-State Experiment

A series of steady-state laboratory tests were conducted to develop a data set that can be compared to the predictions of Eq. (9). This comparison will subsequently be used to assess the validity range for the model. Data obtained by an original set of tests are presented in Ref. 11. Also, additional laboratory data not available when Ref. 11 was originally published will be presented. These additional data will be compared to data taken from Ref. 11.

The test apparatus is shown in Fig. 4. In this series of tests, an evacuated, hermetically sealed oven was used to heat one end of a tube at very low absolute pressure levels. The resulting temperature gradient along the tube induced rarefied gas effects inside of the tube. In this experimental setup, aluminum rods were center bored and an assortment of brass tubes of varying diameters and lengths were press-fit into the resulting holes. The aluminum rods provided a thermal mass to distribute the heat evenly along one the end of the tubing. The cold end of the tube was hermetically bonded to a compression fitting that allowed the heated tube to be accessed from outside the chamber.

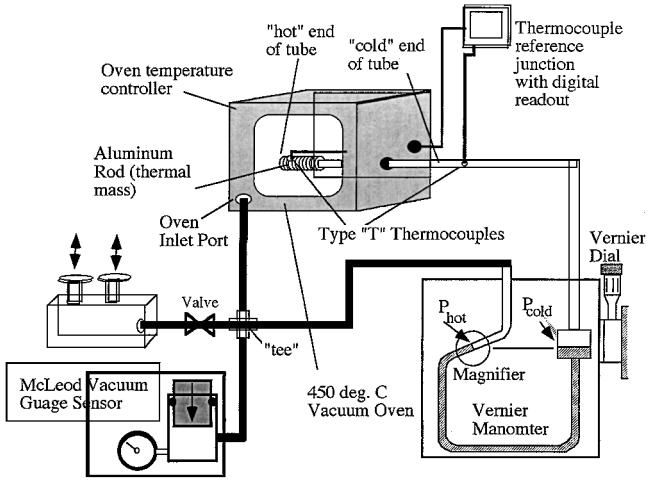

Fig. 4 Schematic of experimental apparatus.

The absolute chamber pressure was measured using a very low pressure sensing device known as a McLeod vacuum gauge.[15] For the McLeod gauge, the manufacturer's (estimated) accuracy specification was approximately 20 μm of mercury (0.0027 kPa). However, repeatability of measurements demonstrated that this uncertainty value was more likely better than 5 μm of mercury (0.0007 kPa).

The differential pressure in the heated tube was measured using a highly sensitive Vernier manometer.[15] The manufacturer's specification for the (estimated) accuracy of the Vernier manometer data was approximately 10 μm of mercury (0.0014 kPa). However, when pre- and posttest zero corrections were applied to the differential pressure data, repeatability showed that the errors were reduced to approximately 2 μm of mercury (0.0003 kPa).

Bimetallic[17] (type T) thermocouple sensors were spot welded to each end of the tube. These thermocouples sensed tube-end temperatures and were used to calculate the longitudinal temperature gradient. At high temperatures, typical accuracies for type T thermocouple measurements are approximately ± 1–2°C. Data repeatability showed that this 1–2°C accuracy level was achieved during these series of tests.

Experiment Uncertainty Analysis

The uncertainty in the normalized Maxwell pressure parameter

$$K_M = \frac{\partial P/\partial x}{P}\Big/\frac{\partial T/\partial x}{T}$$

is formally evaluated using the calculus of variations. Taking the first variation with respect to the components variables gives

$$\Delta\left[\frac{\partial P/\partial x}{P}\Big/\frac{\partial T/\partial x}{T}\right] \approx \Delta\left[\frac{P_{\text{hot}}-P_{\text{cold}}}{P_{\text{hot}}+P_{\text{cold}}}\times\frac{T_{\text{hot}}+T_{\text{cold}}}{T_{\text{hot}}-T_{\text{cold}}}\right]$$

$$= \Delta[P_{\text{hot}}-P_{\text{cold}}]\times\frac{1}{P_{\text{hot}}+P_{\text{cold}}}\times\frac{T_{\text{hot}}+T_{\text{cold}}}{T_{\text{hot}}-T_{\text{cold}}}$$

$$-\Delta[P_{\text{hot}}+P_{\text{cold}}]\times\frac{[P_{\text{hot}}-P_{\text{cold}}]}{[P_{\text{hot}}+P_{\text{cold}}]^2}\times\frac{T_{\text{hot}}+T_{\text{cold}}}{T_{\text{hot}}-T_{\text{cold}}}$$

$$+\Delta[T_{\text{hot}}+T_{\text{cold}}]\times\left[\frac{P_{\text{hot}}-P_{\text{cold}}}{P_{\text{hot}}+P_{\text{cold}}}\times\frac{1}{T_{\text{hot}}-T_{\text{cold}}}\right]$$

$$-\Delta[T_{\text{hot}}-T_{\text{cold}}]\frac{P_{\text{hot}}-P_{\text{cold}}}{P_{\text{hot}}+P_{\text{cold}}}\times\frac{T_{\text{hot}}+T_{\text{cold}}}{[T_{\text{hot}}-T_{\text{cold}}]^2} \tag{11}$$

The variations in Eq. (11) are related to the fundamental measurement errors by Eq. (12):

$$\Delta[P_{\text{hot}}-P_{\text{cold}}] \equiv \delta P_{\text{Vernier}}$$

$$\Delta[P_{\text{hot}}+P_{\text{cold}}] \equiv \delta P_{\text{McLoed}} + \delta P_{\text{Vernier}} \approx \delta P_{\text{McLeod}}$$

$$\Delta[T_{\text{hot}}+T_{\text{cold}}] \approx 2\Delta T, \qquad \Delta[T_{\text{hot}}-T_{\text{cold}}] \approx 2\Delta T_{\text{random}} \tag{12}$$

When Eq. (12) is substituted into Eq. (11), the uncertainty equation becomes

$$\Delta\left[\frac{\partial P/\partial x}{P}\Big/\frac{\partial T/\partial x}{T}\right] \approx \delta P_{\text{Vernier}}\times\frac{1}{P_{\text{hot}}+P_{\text{cold}}}\times\frac{T_{\text{hot}}+T_{\text{cold}}}{T_{\text{hot}}-T_{\text{cold}}}$$

$$-\delta P_{\text{McLeod}}\times\frac{[P_{\text{hot}}-P_{\text{cold}}]}{[P_{\text{hot}}+P_{\text{cold}}]^2}\times\frac{T_{\text{hot}}+T_{\text{cold}}}{T_{\text{hot}}-T_{\text{cold}}}$$

$$+2\Delta T\times\left[\frac{P_{\text{hot}}-P_{\text{cold}}}{P_{\text{hot}}+P_{\text{cold}}}\times\frac{1}{T_{\text{hot}}-T_{\text{cold}}}\right]$$

$$-2\Delta T_{\text{random}}\frac{P_{\text{hot}}-P_{\text{cold}}}{P_{\text{hot}}+P_{\text{cold}}}\times\frac{T_{\text{hot}}+T_{\text{cold}}}{[T_{\text{hot}}-T_{\text{cold}}]^2} \tag{13}$$

The last two terms in Eq. (13) are negligible when compared to the first two terms, and the uncertainty equation is approximated by

$$\Delta\left[\frac{\partial P/\partial x}{P}\Big/\frac{\partial T/\partial x}{T}\right] \approx \left[\frac{\delta P_{\text{Vernier}}}{P_{\text{hot}}+P_{\text{cold}}} - \delta P_{\text{McLeod}} \times \frac{[P_{\text{hot}}-P_{\text{cold}}]}{[P_{\text{hot}}+P_{\text{cold}}]^2}\right] \times \frac{T_{\text{hot}}+T_{\text{cold}}}{T_{\text{hot}}-T_{\text{cold}}} \tag{14}$$

The temperature terms in Eq. (14) simply act as a scaling factor on the certainty. Taking the expectation of the squared uncertainty gives the mean square error in the Knudsen parameter

$$\psi^2\left[\frac{\partial P/\partial x}{P}\Big/\frac{\partial T/\partial x}{T}\right] \approx E\left[\frac{\delta P_{\text{Vernier}}}{P_{\text{hot}}+P_{\text{cold}}} - \delta P_{\text{McLeod}} \times \frac{[P_{\text{hot}}-P_{\text{cold}}]}{[P_{\text{hot}}+P_{\text{cold}}]^2}\right]^2 \left[\frac{T_{\text{hot}}+T_{\text{cold}}}{T_{\text{hot}}-T_{\text{cold}}}\right]^2 \tag{15}$$

When it is assumed that the measurement errors in the McLeod gauge and Vernier manometer are uncorrelated, the mean square error equation reduces to

$$\psi^2\left[\frac{\partial P/\partial x}{P}\Big/\frac{\partial T/\partial x}{T}\right] \approx \frac{1}{[P_{\text{hot}}+P_{\text{cold}}]^2} \times \left[[\delta P_{\text{Vernier}}]^2 + \frac{[\delta P_{\text{McLeod}}]^2}{[P_{\text{hot}}+P_{\text{cold}}]^2}\right]\left[\frac{T_{\text{hot}}+T_{\text{cold}}}{T_{\text{hot}}-T_{\text{cold}}}\right]^2 \tag{16}$$

The root mean square error equation results by taking the square root of Eq. (16):

$$\text{rms}_{\text{error}}\left[\frac{\partial P/\partial x}{P}\Big/\frac{\partial T/\partial x}{T}\right] \approx \left[\frac{T_{\text{hot}}+T_{\text{cold}}}{T_{\text{hot}}-T_{\text{cold}}}\right]\Big/[P_{\text{hot}}+P_{\text{cold}}] \times \sqrt{[\delta P_{\text{Vernier}}]^2 + \frac{[\delta P_{\text{McLeod}}]^2}{[P_{\text{hot}}+P_{\text{cold}}]^2}} \tag{17}$$

The error bounds predicted by Eq. (17) approximate (first-order) $1-\sigma$ uncertainties in the normalized Knudsen pressure parameter K_M.

Experimental Procedures

Because of the extremely low pressure levels at which these series of tests were performed, a systematic set of test procedures was developed to minimize errors introduced by variations in experimental procedure. To minimize the effects of measurement bias in the Vernier manometer a zero-correction procedure was followed. At the beginning of each trial the zero differential pressure in the tube at ambient temperature and pressure was recorded. At the end of each trial, the system was vented and allowed to cool to ambient temperature, and a new zero differential pressure reading was measured. The pre- and posttrial zero readings were averaged and used to correct the differential pressure measurement for bias offsets in the Vernier manometer.

Once the pretrial bias readings were recorded, the oven-chamber heater was activated with the required temperature setting selected on the thermal controller. The chamber was evacuated to the desired pressure, and the system was allowed to thermally stabilize. For each trial, once a stable temperature was reached, the temperature setting was maintained constant, and the chamber pressure was systematically lowered starting from the highest desired pressure level and working toward the lowest desired pressure level. For each oven-temperature setting, approximately 30 pressure levels were tested. At each pressure setting, once a stable pressure and temperature was achieved, the vacuum pump was shut down and sealed off. The chamber was allowed to settle, and the hot- and cold-end temperatures were recorded using the thermocouples. At this point the absolute chamber pressure was recorded using the McLeod gauge, and the differential pressure in the tubing was recorded using the Vernier manometer.

Data Summary

As mentioned earlier, this paper presents steady-state test data not available when Ref. 11 was published. The previously unpublished test data are summarized in Fig. 5, where the average of the hot- and cold-end tube pressures are plotted against κ_0 (Knudsen number calculated by averaging hot- and cold-end pressure and temperature values). Four different tubing diameters, 0.071 (0.028), 0.16 (0.063), 2.14 (0.84), and 2.34 cm (0.92 in.), were tested. The minimum pressure levels achieved for these series of tests are significantly lower than those achieved in Ref. 11. The minimum pressure levels achieved in Ref. 11 were on the order of 100 μm of mercury

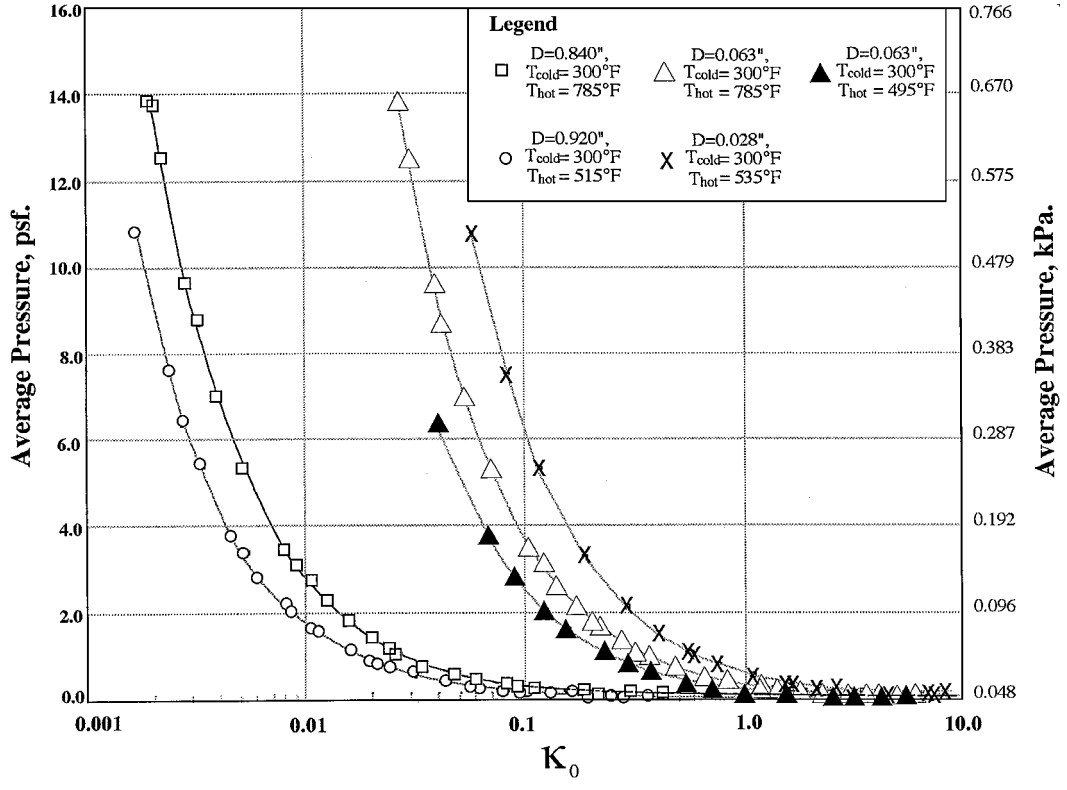

Fig. 5 Summary of steady-state test conditions.

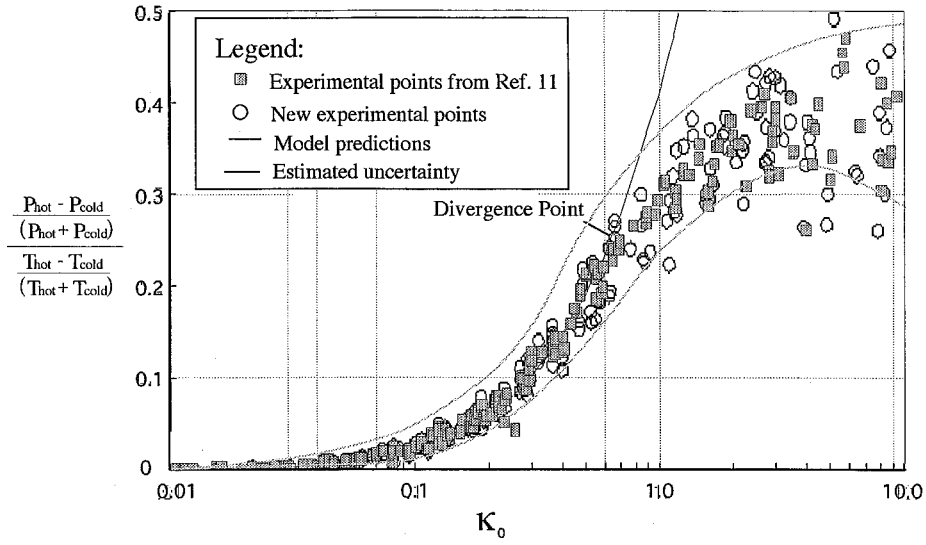

Fig. 6 Comparison of the steady-state model response to experimental results.

(0.014 kPa). For these tests, modifications to the vacuum seal of the oven chamber allowed pressures as low as 15 μm of mercury (0.002 kPa) to be achieved. The resulting values for Knudsen number varied from effectively zero to approximately 10. The vacuum oven provided sufficient heating to allow temperature gradients as high as 1340°C/cm to be achieved. The tube endpoint temperatures achieved in this series of tests are summarized in Fig. 5.

Experiment Results

When Eq. (9) is used as a guide, the Maxwell pressure parameter is approximated by dividing the normalized pressure differential by the normalized temperature differential:

$$K_M = \frac{\partial P/\partial x}{P} \Big/ \frac{\partial T/\partial x}{T} \approx \left[\frac{P_{\text{hot}} - P_{\text{cold}}}{(P_{\text{hot}} + P_{\text{cold}})/2} \Big/ \frac{T_{\text{hot}} - T_{\text{cold}}}{(T_{\text{hot}} + T_{\text{cold}})/2} \right] \tag{18}$$

This data normalization allows the experimental data to be collapsed into a single curve by plotting the result as a function of κ_0. The normalized test data are plotted in Fig. 6 along with the model steady-state predictions, the error bounds predicted by Eq. (17), and experimental data originally published in Ref. 11. Several observations can be made with regard to Fig. 6:

1) The new experimental results show excellent agreement with regard to the originally published experimental data taken from Ref. 11. The relatively larger scatter at the higher Knudsen numbers is a result of the relatively lower absolute pressure levels achieved during these tests.

2) The approximate error analysis of Eq. (17) is conservative. For Knudsen numbers below 2, the data repeatability shows that the true measurement error is significantly better than the theoretical error bound. The relatively larger amount of scatter at higher Knudsen numbers is a result of the very low absolute pressure levels used in the data normalization.

3) The steady-state model matches the data extremely well for Knudsen numbers up to approximately 0.65. In this flow regime the slip-flow equations used in deriving the dynamic model appear to be completely valid.

Beyond $\kappa_0 > 0.7$, the curves rapidly diverge. The most likely cause of this divergence is that molecular effects begin to dominate, and continuum flow no longer exists in the center of the tube. This divergence point is labeled in Fig. 6. This divergence point marks the upper bound on the model's usefulness. Fortunately, it appears that the model is valid for most of the slip-flow data regime.

Summary

This paper reports on the development of a dynamic model for pressure sensing configurations in slip-flow conditions. The model represents a fundamental extension to the understanding of flow behavior at the limits of the continuum-flow regime. Rarefied gas effects manifest themselves in two ways:

1) At very low pressure levels, the low molecular density allows the fluid to slip at the tubing wall. The end result is that the fluid viscosity is effectively lowered, and the dynamic response of the tubing configuration is less damped than would occur if molecular effects were negligible. The fluid motion at the wall boundary allowed by the rarefied conditions has the effect of reducing the viscosity.

2) Under steady flow conditions where the tube is heated unevenly, the hot end of the tube has a higher average cross-sectional pressure than does the coldend of the tube, with no net flow in the tube. This pressure bias manifests itself as a dc offset in the measured pressure reading.

The applicable flow regimes for the model were evaluated by a series of steady-state laboratory tests. Model comparisons are excellent for Knudsen numbers up approximately 0.65. For values of $\kappa_0 > 0.7$, free-molecule effects dominate, and the model is no longer valid. The model allows instrumentation designers to evaluate the responses of pneumatic systems over a wide range of flow conditions, which may vary continuously from continuum to slip flow. Other potential applications outside of aerospace include predicting the behavior of micromachined fluid systems where the mean free path of the working fluid is on the order of the channel diameter.

References

[1]Lamb, R. C., "The Influence of Geometry Parameters upon Lag Error in Airborne Pressure Measurement Systems," Wright Air Defense Center, TR 57-351, Wright–Patterson AFB, OH, July 1957.

[2]Iberall, A. S., "Attenuation of Oscillatory Pressures in Instrument Lines," U.S. National Bureau of Standards, Rept. RP 2115, Vol. 45, Washington, DC, Jan. 1950.

[3]Schuder, C. B., and Binder, R. C., "Response of Pneumatic Transmission Lines to Step Inputs," *Journal of Basic Engineering*, Vol. 81, No. 12, 1959, pp. 578–584.

[4]Hougen, J. O., Martin, O. R., and Walsh, R. A., "Dynamics of Pneumatic Transmission Lines," *Journal of Control Engineering*, Vol. 10, No. 3, 1963, pp. 114–117.

[5]Berg, H., and Tijdeman, H., "Theoretical and Experimental Results for the Dynamic Response of Pressure Measuring Systems," Nationale Luchtavaatlab, NLR TR F.238, Amsterdam, Jan. 1965.

[6]Tijdeman, H., "Investigation of the Transonic Flow Around Oscillating Airfoils," Nationale Luchtavaatlab, NLR TR 77090 U, Amsterdam, Aug. 1977.

[7]Parrot, T. L., and Zorumski, W., "Sound Transmission Through a High-Temperature Acoustic Probe Tube," *AIAA Journal*, Vol. 30, No. 2, 1992, pp. 318–323.

[8]Maxwell, J. C., "On Stress in Rarefied Gases Arising from Inequalities of Temperature," *Journal of Philosophical Transactions*, Vol. 170, Pt. I, Jan. 1879, pp. 231–235.

[9]von Knudsen, M., "Eine Revision der Gleichgewichtsbedingung der Gase: Thermische Molekularströmung," *Annalen dek Physik*, Vol. 31, Nov. 1910, pp. 205–229.

[10]Tompkins, J., and Wheeler, L., "The Correction for Thermo-Molecular Flow," *Transactions of the Faraday Society*, Vol 29, No. 1, 1933, pp. 1248–1254.

[11]Whitmore, S. A., Petersen, B. J., and Scott, D. D., "A Dynamic Response Model for Pressure Sensors in Continuum and High Knudsen Number Flows with Large Temperature Gradients," NASA TM-4728, Jan. 1996.

[12]Kennard, E. H., *Kinetic Theory of Gases*, 1st ed., McGraw–Hill, New York, 1938, pp. 311–337.

[13]Stephens, R. W. B., and Bate, A. E., *Acoustics and Vibrational Physics*, 1st ed., St. Martin Press, New York, 1966, pp. 660–682.

[14]Freiberger, W. F. (ed.), *The International Dictionary of Applied Mathematics*, 1st ed., D. Van Nostrand, Princeton, NJ, 1960, p. 707.

[15]Doebelin, E. O., *Measurement Systems Application and Design*, 3rd ed., McGraw–Hill, New York, 1983, pp. 410–455.

[16]Rade, L., and Westergren, B., *Beta Mathematics Handbook*, 2nd ed., CRC Press, Boca Raton, FL, 1990, pp. 287, 288.

[17]Holman, J. P., *Experimental Methods for Engineers*, 3rd ed., McGraw–Hill, New York, 1978, pp. 280–282.

I. D. Boyd
Associate Editor